Fundamentals of high-energy electron-irradiation-induced modifications of silicate glasses

Nan Jiang*
Department of Physics and Astronomy, Arizona State University, Tempe, Arizona 85287, USA and School of Applied and Engineering Physics and Cornell Center for Materials Research, Cornell University, Ithaca, New York 14853, USA

Jianrong Qiu
Photoncraft Project, JST, Keihanna-Plaza, Seika-cho, Kyoto 619-0237, Japan

Adam Ellison
Corning Inc., Corning, New York 14831, USA

John Silcox
School of Applied and Engineering Physics and Cornell Center for Materials Research, Cornell University, Ithaca, New York 14853, USA
(Received 27 January 2003; revised manuscript received 5 May 2003; published 26 August 2003)

We report *in situ* observations of modifications in silicate glasses using electron-energy-loss spectrometry with a small-probe (2.2 Å) scanning transmission electron microscope. Two silicate glasses $CaO\text{-}Al_2O_3\text{-}SiO_2$ and $ZnO\text{-}B_2O_3\text{-}SiO_2$ are examined. It is found that the nonbridging oxygen (NBO) in glasses plays a critical role in irradiation phenomena. We suggest that a highly localized density of states on the NBO's probably results in a very high sensitivity to electron irradiation of the cations bound to NBO's. These irradiation phenomena noted above reflect a tendency of electron irradiation to eliminate NBO's in the irradiated region.

DOI: 10.1103/PhysRevB.68.064207 PACS number(s): 79.20.Uv, 61.80.Fe, 61.82.Ms

I. INTRODUCTION

Irradiation effects in glasses have attracted much study,[1] since they not only affect the interpretation of experimental results associated with glasses, but also promise an efficient approach to modify the electronic and optical properties of glasses. Recently, the precipitations of nanometer metallic particles induced by electron irradiation have been reported in Zn borosilicate glasses[2] and Cu-doped SiO_2 (Ref. 3). The existence of nanometer particles may improve the nonlinear optical properties of these glasses.[4] There is also evidence showing that nanoscale modification of the optical properties in Ge silicate glasses can be obtained by a high-energy electron beam.[5] Various mechanisms have been introduced to interpret irradiation effects in glasses, such as ion migration, phase decomposition, gas bubble formation, and even crystallization in different glasses.[6] Two broad categories of processes—i.e., radiolysis (ionization and electronic excitation processes) and knock-on (elastic) collisions—are involved in high-energy electron-solid interactions. However, the fundamental understanding of irradiation mechanisms in glasses at the atomic level is limited and is highly desirable in order to predict modification by electron beams.

Over several decades of studies, there is no doubt concerning the O_2 evolution in electron-irradiated silicate glasses.[7–9] It is suggested that the migration of cations from the center of the irradiated region to the periphery may be relevant to the liberation of oxygen, hence leading to the nucleation of gas bubbles.[10,11] The cations might diffuse to the sites of trapped electrons, thus forming neutralized clusters.[12] Many techniques have been used to examine the post-irradiated silicate glasses.[13,14] Recently, direct *in situ* observation of electron-irradiated SiO_2 polymorphs has also been reported.[15] *In situ* data in silicate glasses, however, are limited, although *in situ* observation using x-ray photoelectron spectroscopy (XPS) has been reported.[16] In this article, we present our recent studies on irradiation effects in silicate glasses by *in situ* electron-energy-loss spectroscopy (EELS) in the electron microscope and discuss the fundamental mechanisms of the interactions of high-energy electrons with silicate glasses at atomic level.

In EELS, fast electrons that lose characteristic amounts of energy to electronic excitations in electron-irradiated materials are recorded by an electron spectrometer. It has developed into an established technique for chemical analysis, and electron-energy-loss near-edge fine structure (ELNES) in core edges has also been used to probe the electronic structure of materials.[17,18] Recently, there has been substantial interest in applying ELNES to obtain the local structural environment of the atom undergoing an electron excitation.[19] Briefly, the idea is that EELS probes the unoccupied local density of states (LDOS), which is mainly determined by the short-range order if short-range interactions between electrons are dominant.[20] For example, the EELS of the Si L_{23} edges have similar ELNES in many SiO_2-related materials,[21] in which the Si have the same nearest neighbors. The calculated electronic structures of both crystalline and amorphous SiO_2 are also roughly similar, although there are differences in detail.[22] So EELS can promise *in situ* studies of electron-irradiation-induced changes in the local structure, chemistry, and electronic density of states, thus revealing the fundamental mechanisms of electron irradiation effects. In combination with electron microscopy, providing high spatial resolution, it is also possible to achieve simultaneous records of both EELS and image signals.

II. EXPERIMENT

Two silicate systems have been used in this study; they are calcium aluminosilicate ($42CaO\text{-}25Al_2O_3\text{-}33SiO_2$) and zinc borosilicate ($60ZnO\text{-}20B_2O_3\text{-}20SiO_2$) (in mol %) glasses, respectively. Electron microscope specimens were prepared by grinding the glass into a powder in acetone and mounting suspended pieces on a holy-carbon-film-covered copper grid. The sizes of glass particles are in the range of 20–100 nm. This has the advantage that there is less contamination on glass surfaces. The glasses used in this study are visually homogeneous; no phase separation has been observed in the initial electron irradiation.

The glasses were observed and analyzed in the Cornell VG HB501 100 kV UHV scanning transmission electron microscope (STEM), equipped with an annular dark field (ADF) single-electron sensitivity detector[23] and a parallel electron-energy-loss spectrometer.[24] The attainable electron probe size in the Cornell STEM is about 2.2 Å in full width at half maximum (FWHM), and the saturated current intensity of the probe is about 0.3 nA. The energy stability of the spectrometer is about 0.03 eV/min, and the energy resolution of EELS is about 0.7 eV. More details of this instrument can be found elsewhere.[25] The pressure in the microscope was 10^{-10} Torr, and no specimen contamination from carbon was detected during experiments.

Basically, two illumination modes can be achieved in the STEM: a scanning mode and a spot mode. In the scanning mode or called the *area* mode, the subnanometer electron probe is scanned either along a line (for instance, an illuminating area of about 2.2 Å$\times$1280 Å) or across an area (e.g., 1280 Å$\times$1280 Å in area) on the specimen to generate EELS signals. This reduces the influence of irradiation effects. In the *spot* mode, the electron is fixed on a selected location (about 2 Å$\times$2 Å in area) controlled by a computer. Incident electrons are precisely concentrated in a small region (no more than 5 Å$\times$5 Å in area including beam broadening effect[26]) and thus can probe physics and chemistry properties on a subnanometer scale. Obviously, a small probe is essential in studies of irradiation effects. For instance, diffusion on a nanometer scale induced by irradiation is then detectable, which is crucial for understanding probe and specimen interactions. From the macroscopic point of view, positive charges can be built up in insulator materials by electron and x-ray irradiation.[27] The charging effects usually cause the sample drift in TEM. Practically, the drift can be minimized in the STEM with the use of a subnanometer probe. This is probably because using a subnanometer probe in STEM, cations may easily move into the adjacent region; therefore, neutrality is restored within the probe.[28]

The results of this study largely rely on the EELS of the O *K* edge. In addition, the EELS of the Ca L_{23}, Al L_{23}, and Si L_{23} edges are also observed. A simple model of single-electron transitions can be used to interpret the deep core-shell excitations, since many-body effects can be treated as perturbations to the single-particle transitions.[29] In a solid, the unoccupied states result from the interactions of the outer orbital of atoms and thus are a mixture of atomic states. Restricted by the dipole selection rules ($\Delta l = \pm 1$) for small momentum transitions,[30] the EELS of the O *K* edge probes the unoccupied states with O $2p$-like symmetry, while the L_{23} edges in Ca, Al, and Si project the *s*-like and *d*-like states. In experiments, all the energies of the core-level ionization have been scaled to the π^* peak at 284 eV of the C *K* edge in amorphous carbon thin films. The backgrounds of the spectra have been properly fitted and subtracted from the original EELS data. No deconvolution has been done to correct the multiple scattering, since it does not have a large effect on the near-edge structures.[31]

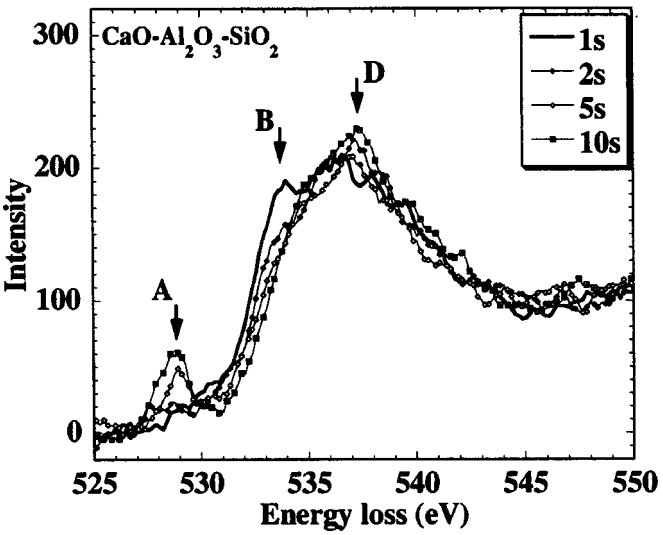

FIG. 1. *In situ* EELS of the O *K* edge in the *spot* mode with dose rate of 2×10^4 C/cm^2 sec. The high-voltage stability has been confirmed by comparing the peak positions of the π^* in the C *K* edge in amorphous carbon thin film before and after recording these spectra.

III. RESULTS

A. Variations of ELNES in $CaO\text{-}Al_2O_3\text{-}SiO_2$ glass

The *in situ* ELNES of the O *K* edges are shown in Fig. 1, in which the spectra were generated using the *spot* mode (with an electron probe current intensity of ~0.03 nA), and the estimated electron dose rate is about 2.0×10^4 C/cm^2 sec. No effort has been done to align the intensities of these time-resolved spectra to any reference. Two significant changes are seen: the drop of the intensity around 533.7 eV (marked as peak *B*) and the appearance of the peak at ~528.8 eV (marked as peak *A*). Peak *B* drops dramatically in the first 2 sec of irradiation and continuously decreases with electron irradiation. As a result, the threshold of the O *K* edge shifts toward high energy after 10 sec of irradiation. On the contrary, peak *A* does not appear until after 5 sec of irradiation, and it increases in 10 sec. In addition, several minor changes are also seen in Fig. 1. For instance, the intensity at 537.9 eV (indicated as peak *D*) increases gradually with electron irradiation and finally forms a significant peak after 10 sec.

The *in situ* EELS of the Ca L_{23} edges in this glass have also been observed under the same conditions as in Fig. 1 and are shown in Fig. 2. It is seen that the ELNES of the Ca

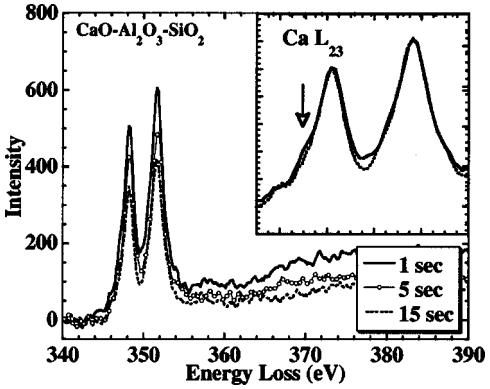

FIG. 2. *In situ* EELS of the Ca L_{23} edge in the *spot* mode with dose rate of 2×10^4 C/cm^2 sec. The inset is a comparison of two spectra recorded at 1 and 15 sec, respectively, which are scaled to the same height of the first peak.

L_{23} edge has little change during the irradiation, but the intensity drops significantly.

The time-resolved total intensities of the Ca L_{23} and O *K* edges and the relative intensities of peaks *A* and *B* to the total intensity of the O *K* edge, as well as the ADF intensities (recorded simultaneously with the EELS spectra) are plotted

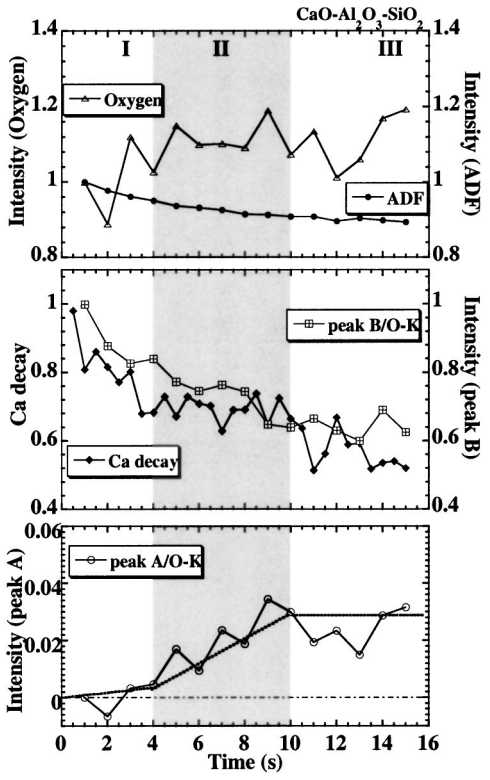

FIG. 3. Intensity variations of the O *K* and the corresponding ADF signal (on the top), Ca L_{23} edges and peak *B* (in the middle), and peak *A* (on the bottom) vs irradiation time. The illumination conditions are the same as in Figs. 1 and 2. The intensity of the O *K* edge is integrated over the first major peak (525–550 eV), and that of the Ca L_{23} edge is over both L_3 and L_2 peaks. The intensities of peaks *A* and *B* are scaled to the intensity of the O *K* edge. The dotted line is a guide for the eyes.

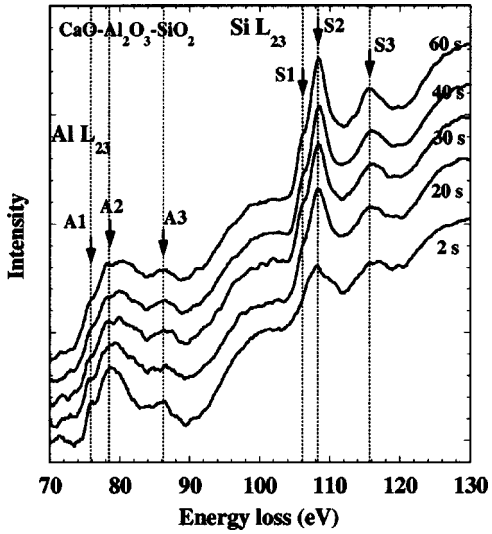

FIG. 4. *In situ* EELS of the Al L_{23} and Si L_{23} edges in the *spot* mode with dose rate of 2×10^4 C/cm^2 sec.

in Fig. 3. (The EELS intensities, throughout this paper, are normalized to the first observation.) Although the data are scattered due to the low signal-to-noise ratio, the O intensity exhibits an increasing trend, which is unexpected in terms of the knock-on damage mechanism since oxygen is the lightest element in the glass. It is noted that the decay of the EELS intensity of peak *B* in the O *K* edge seems related to the decay of the Ca; both the Ca concentration and peak *B* in the O *K* edge decrease rapidly. About half of the calcium is left after 16 sec of irradiation while the intensity of peak *B* disappears. It should be noted that peak *B* accidentally shows a similar decay rate to the Ca due to an arbitrary selection of the energy windows for integrating the intensity of peak *B*. The intensity from the pre-edge tails of other peaks (such as peak *C*) may contribute to the integrated results. It is seen that the variation of the EELS intensity of peak *A* is significantly different from that of peak *B*. Peak *A* does not exist until after a certain initial amount of irradiation. Then there is a short period during which the intensity of peak *A* increases with irradiation, and after that the intensity remains approximately constant.

The decay in the ADF intensity may reflect the loss of mass in the irradiated region. However, the decay rate of the Ca, the heaviest element in the glass, is much larger than that of the ADF intensity.[32] In other words, the loss of Ca must be compensated by other species that diffuse into the irradiated region.

The *in situ* ELNES of the Al and Si L_{23} edge under the same experimental conditions as in Figs. 1 and 3 are shown in Fig. 4. The Al L_{23} edge shows little changes within 20 sec, which is twice longer than the observation period of the O *K* edge in Fig. 1 (10 sec). Peaks *A*1, *A*2, and *A*3 can always be recognized. Although the Si L_{23} edge is on the tail of the Al *L* edge, the ELNES of the Si L_{23} edge do show significant changes within 20 sec of electron irradiation. After the electron irradiation, the amorphous SiO_2-like features become more and more distinct: peak *S*1 at 106 eV (Ref. 33) can be recognized, peak *S*2 at 108.3 eV becomes narrower and

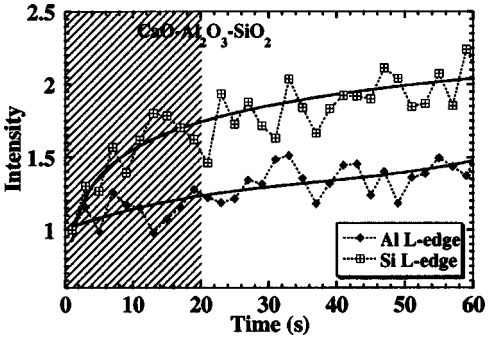

FIG. 5. Intensity variations of the Al L_{23} and Si L_{23} edges vs irradiation time. The illumination conditions are the same as in Fig. 4. Solid lines are guides for eyes. The hatched area indicates the same irradiation period as that in Fig. 3.

sharper, and the peak at 117 eV disappears, leaving a single peak ($S3$) at 116 eV (Ref. 34). After a long time of irradiation (60 sec), however, an extra peak (indicated by an arrow) at about 80 eV appears in the Al L_{23} edge and the threshold energy of the Al L_{23} edge shifts towards low energy. The ELNES of the Si L_{23} edge becomes more and more a-SiO_2 like.

The corresponding variation of the total intensities of the Al L_{23} and Si L_{23} edges is given in Fig. 5. It should be noted that the intensity of the Si L_{23} edge includes the background from the tails of the Al L_{23} edge, which is difficult to be subtracted. The results in Fig. 5 are obtained by dividing the total intensity under the Si L_{23} edge (in Fig. 4) by the integrated intensity of the Al L_{23} edge with the same energy window. Therefore the resulting curve in Fig. 5 approximately represents the Si variation trend. As shown in Fig. 5, the EELS intensity of the Si increases rapidly within 20 sec of irradiation and that of the Al has a slow increase. In a brief summary, the illuminated region loses Ca, but gains all other elements during the electron irradiation within the initial observation period.

By increasing the beam current to 0.3 nA (at the saturated extraction voltage)—i.e. an electron dose rate of 2.0×10^5 C/cm^2 sec—Fig. 6 shows the dramatically changed ELNES of the O K edge by electron irradiation. The acquisition of the first spectrum (labeled as 0.5s) was started in an undamaged area. The irradiation time is considered to be approximately identical with the acquisition time of the spectrum. So in terms of electron dose, the first spectrum should be similar to the spectrum with 5 sec of irradiation in Fig. 1, and they are indeed almost identical. In other words, operating the (S) TEM under normal conditions, the observed spectrum within a certain acquisition time (such as 0.5 sec in the CaO-Al_2O_3-SiO_2 glass) might not always reflect the original features of irradiation-sensitive materials.

As shown in Fig. 6, the variation of the ELNES of the O K edge during electron irradiation is significant. Peak A initially increases with electron irradiation, but then decreases rapidly after 4 sec of irradiation and eventually disappears after about 6 sec. Referring to its appearance in Figs. 1 and 6, creating and annihilating peak A are purely electron irradiation effects. The width of peak A is about 2 eV, which does

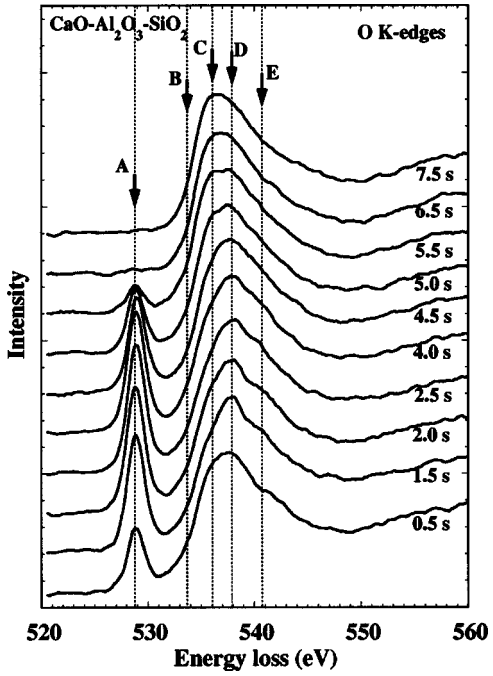

FIG. 6. *In situ* EELS of the O K edge in the *spot* mode with dose rate of 2×10^5 C/cm^2 sec.

not change during the electron irradiation. Meanwhile, the intensity of peak B continuously decreases and becomes negligible as peak A disappears. The intensity at about 536.1 eV gradually increases and becomes the dominant peak (indicated as peak C) after 6.5 sec of irradiation (as peak A disappears). The changes of peak D are the same as those of peak A. It also disappears as peak A disappears. In addition, there is a small bump at about 541.4 eV (indicated as peak E), whose change is also associated with that of peak A. All the peaks in the O K edge and their changes are summarized in Table I. Obviously, peaks A, D, and E have the same variation, but peak B decreases while peak C increases during the electron irradiation.

In brief, five stages can be distinguished during continuous electron irradiation of the glass. In the first stage, no peak A in the O K edge occurs, but peak B dramatically drops (with Ca). In the second stage, peak A increases rapidly with electron irradiation, while peak B continuously decreases. After the second stage, peak A has a relatively constant (saturated) intensity, while peak B disappears. In the fourth stage, the intensity of peak A decreases during further irradiation. With continuous irradiation, peak A will disappear completely and this is the fifth stage.

B. Variations of ELNES in ZnO-B_2O_3-SiO_2 glass

It was found in this study that the ZnO-B_2O_3-SiO_2 glass is much more sensitive to electron irradiation than is the CaO-Al_2O_3-SiO_2 glass. Milliseconds of irradiation at the rate of 2.0×10^5 C/cm^2 sec will dramatically alter the glass structure. To generate high signal-to-noise ratio spectra, all the observations in this glass are carried out in the *area* mode at the saturated extraction voltage (probe current is 0.3 nA). The scanned area is divided into a certain number of pixels

TABLE I. Summary of the subpeaks in the O K edge in the $CaO\text{-}Al_2O_3\text{-}SiO_2$ and $ZnO\text{-}B_2O_3\text{-}SiO_2$ glass, intensity variations vs irradiation time, and their assignments. The upward and downward arrows represent increase and decrease, respectively.

$CaO\text{-}Al_2O_3\text{-}SiO_2$					
Peak	A	B	C	D	E
Energy (eV)	528.8	533.7	536.1	537.9	541.4
Variation	↑ then ↓	↑	↓	↑ then ↓	↑ then ↓
Assignment	$O_2(\pi^*)$	NBO	BO	O_2	O_2
$ZnO\text{-}B_2O_3\text{-}SiO_2$					
Peak	A	B	C	D	E
Energy (eV)	528.7	533.6	533.6	536.5	543.5
Variation	↑ then ↓	↑	↓	↓	↑
Assignment	$O_2(\pi^*)$	NBO	$B_2O_3(\pi^*)$	SiO_2	B_2O_3

(e.g., 256×256), and the 0.1-msec exposure time of each pixel (dwell time) is set up by the computer software. For the sake of accuracy, the pixel dimension should match the probe size. So the irradiation time should be approximately equal to the total exposure time of each pixel. It should be noted that each pixel is not exposed to an electron beam continuously in the area mode. The ''relaxation'' may have an effect on the observations, but the main irradiation effects are dominant in the *in situ* spectra. This is because most irradiation-induced phenomena are irreversible.

Figure 7 shows the *in situ* EELS of the O *K* edge in the $ZnO\text{-}B_2O_3\text{-}SiO_2$ glass. For comparison, all spectra have been scaled to the intensity of the first major peak from 530 to 550 eV. Two significant changes are seen in Fig. 7: peak *B* decreases rapidly and continuously during irradiation, along with the occurrence and then disappearance of peak *A*. It is seen that peak *B* eventually disappears and thus results in shifts of the threshold of the O *K* edge toward high energy. In addition, three peaks (marked as peaks *C*, *D*, and *E*) can be recognized in the last spectrum (6.0 msec) in Fig. 7. It should be noted that peaks *B* and *C* in Fig. 7 are at the same energy position, but have different origins. This is obtained from decomposing the O *K* edge after damage into components of O *K* edges in B_2O_3 and SiO_2 (see later discussion).

The intensity variation of peaks *A* and *B* during irradiation is shown in Fig. 8, as well as that of the total intensity of the O. In fact, the intensity curve of peak *B* should be separated into two parts. The first part of the curve is dominated by the variation of peak *B* and reflects its monotonic decrease with irradiation, and the second part should be mainly a contribution from peak *C* (see later discussion). This is because both

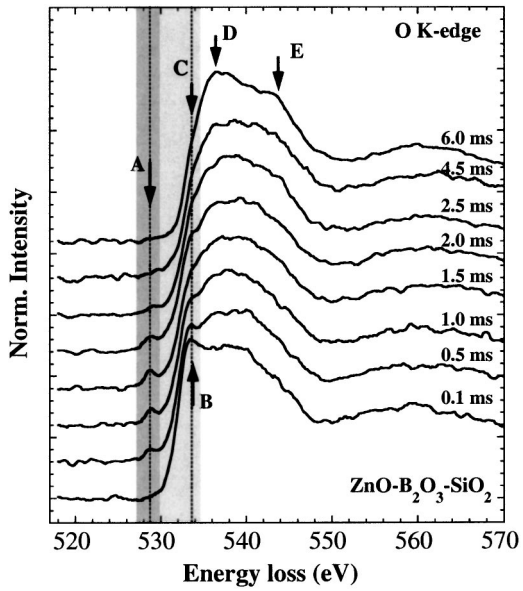

FIG. 7. *In situ* O *K* edge in the Zn borosilicate glass. The shaded areas denote the integration windows of energy for peak *A* (darker) and peak *B* (lighter).

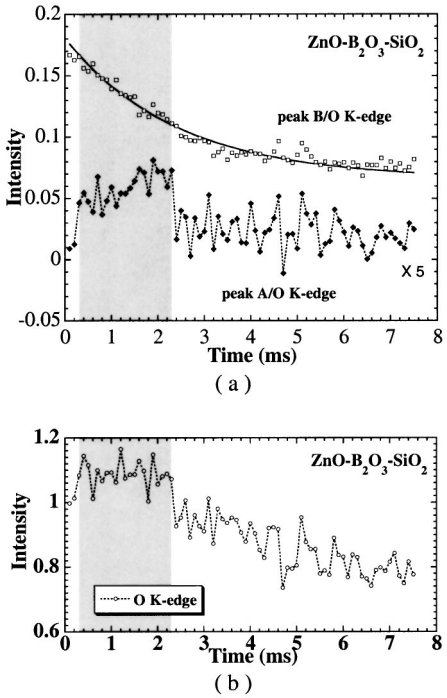

FIG. 8. Variation of the relative intensities of peaks *A* and *B* [in (a)] and the O *K* edge [in (b)] vs irradiation time. The shaded area indicates the period of appearance of peak *A*.

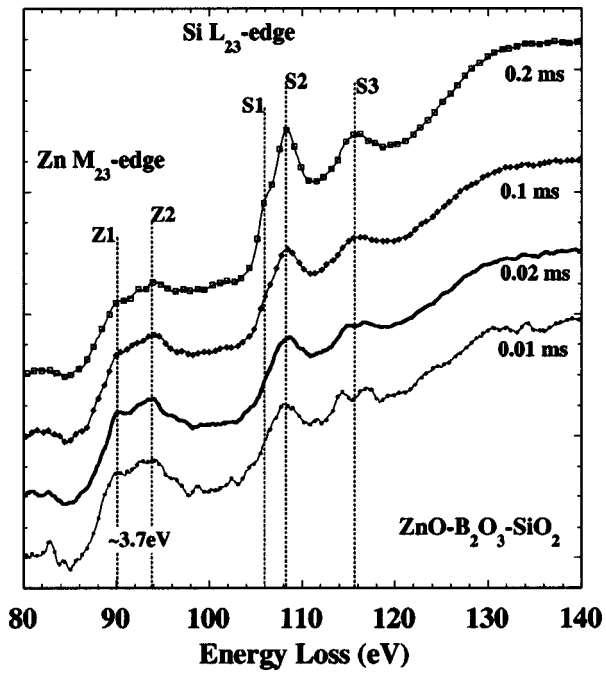

FIG. 9. *In situ* EELS of the Zn M_{23} and Si L_{23} edges in the Zn borosilicate glass. Several reproducible and distinct features are indicated.

peaks are within the integration energy windows. The separation lies between 2.5 and 3.0 msec, but it is difficult to draw a line precisely. Nevertheless, peak *B* can be considered to disappear within 3 msec of irradiation. The subsequent decrease of the curve (after 3 msec) should be the variation of peak *C*. Peak *A* does not exist initially; it is created by irradiation after about 0.3 msec and remains approximately constant until after 2.3 msec of irradiation. However, further irradiation destroys the peak. It is noted that the variation of peak *A* is very similar to that of the O intensity [Fig. 8(b)]. The O intensity initially increases and remains a constant until 2.3 msec of irradiation. Then it continuously decreases with further irradiation. In general, irradiation-induced changes in the O *K* edge in the ZnO-B_2O_3-SiO_2 glass are similar to those in the CaO-Al_2O_3-SiO_2 glass (Fig. 3).

The ELNES of the Si L_{23} edge in the ZnO-B_2O_3-SiO_2 glass show dramatic changes under electron irradiation (Fig. 9). The changes are similar to those in the CaO-Al_2O_3-SiO_2 glass (Fig. 4); the amorphous SiO_2-like characteristics (peaks *S*1, *S*2, and *S*3) become more and more distinct. At the beginning of irradiation, the Si L_{23} edge has distinct features such as the two peaks marked by arrows around 116 eV. (The origin of these peaks is not investigated in this study.) With increasing electron dose, these two peaks become closer and eventually merge as one peak (*S*3) at 116 eV. The Zn M_{23} edge also changes with electron irradiation, but the ELNES of the Zn M_{23} edge are not fully understood yet. Two peaks (*Z*1 and *Z*2) may result from orbital-spin splitting of the $3p_{1/3}$ and $3p_{2/3}$ states.[35]

The origin of peaks *C*, *D*, and *E* can be understood by decomposing the O *K* edge after 6.0 msec of irradiation in Fig. 10. The spectrum from a mixed oxide with 40 mol % of B_2O_3 and 60 mol % of SiO_2 fits very well with that in the

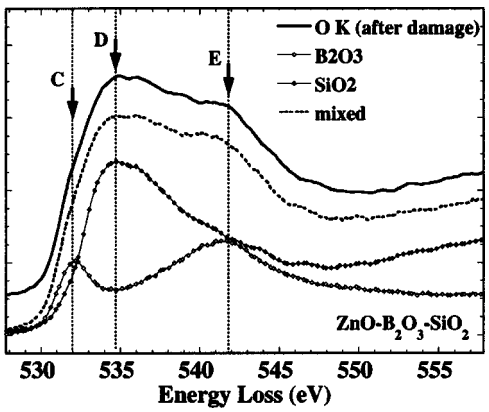

FIG. 10. Decomposition of the O *K* edge after irradiation damage. The energy has been scaled to the π^* peak (284 eV) of the amorphous C film.

damaged glass. In B_2O_3, the B is coordinated to three oxygen atoms, so the first peak is from an antibonding π^* orbital and the second broad peak is from an antibonding σ^* (Ref. 36). As a result, we can assign peaks *C* and *E* to the π^* and σ^* peaks of the B-O trigonal, respectively, and peak *D* to the Si-O tetrahedron. It should be noted that with the added ZnO, the B would likely be in fourfold coordination. Therefore the observed peaks *C*, *D*, and *E* are the products of irradiation, in which peak *C* is accidentally coincident with peak *B*. In the original glass, the B_2O_3 and SiO_2 have the same amount (50:50), but the B_2O_3 becomes less than the SiO_2 (40:50) after irradiation. This suggests that the B_2O_3 is more unstable under electron irradiation than the SiO_2. Thus, as mentioned above, the decrease of peak *C* may result from the breaking of B-O bonding in the B_2O_3 caused by electron irradiation.

If the EELS of the O *K* consist of only Si-O and B-O interactions after irradiation, where is the Zn-O component? In fact, the Zn ions in the glass have been neutralized and

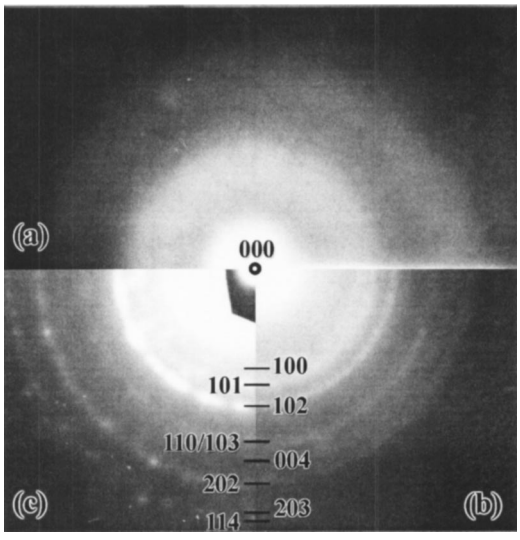

FIG. 11. Time-resolved electron diffraction patterns from Zn borosilicate glass. They were taken one after another. The exposure time of each is 0.2 sec.

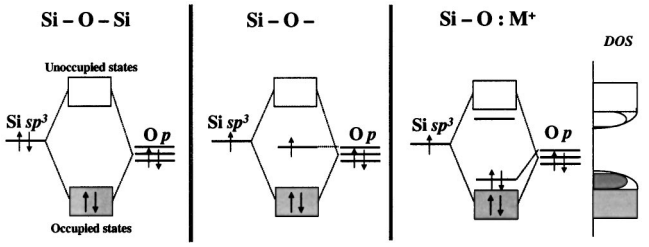

FIG. 12. Schematic drawing of the origin of occupied and unoccupied DOS on NBO in silicate glassed. The left panel is the case of continuous Si tetrahedra. The middle panel is a Si tetrahedron with on dangling bonded O. In the right panel, a cation is bound to this dangling-bonded O.

have precipitated into nanometer-scale metallic particles.[2] Time-resolved diffraction patterns are shown in Fig. 11. Figure 11(a) is the diffraction pattern of the glass at the beginning of electron irradiation. It is typical of an amorphous material. Then crystallization occurs as seen in Fig. 11(b). As the electron dose increases, the crystalline particles grow, and diffraction spots can be seen in Fig. 11(c). The indices of the diffraction rings are consistent with metallic Zn. This conclusion—that the crystalline particles consist of metallic Zn—is also confirmed from EELS analysis in the low-energy-loss range ($<$40 eV). The size of the particles is about 7 nm. More details can be found in Ref. 2.

The formation of the Zn particles in the Zn borosilicate by irradiation is extremely efficient. Within 6 msec of irradiation, almost all 60 mol % of ZnO has been converted into metallic Zn. According to the results shown in Fig. 10, no Zn is bonded to O after 6.0 msec of irradiation. It should be noted that thermal effects could be excluded from the interpretation. This is because the normal annealing temperature of the Zn borosilicate glass is about 600 °C (Ref. 37), which is higher than the melting temperature of Zn [about 400 °C (Ref. 38)].

IV. DISCUSSION

A. O *K*-edge ELNES before and after irradiation damage

Experimental spectra from the compositionally equivalent crystals may help understand these O *K* edges in the glasses, but no such crystals exist in either of form $42CaO\text{-}25Al_2O_3\text{-}33SiO_2$ or $60ZnO\text{-}20B_2O_3\text{-}20SiO_2$. Nevertheless, the O *K* ELNES has been successfully decomposed into contributions from the Si-O (NBO), Si-O-Si, and Si-O-Al configurations in the $42CaO\text{-}25Al_2O_3\text{-}33SiO_2$ glasses based on multiple-scattering calculations in a modified crystalline form.[39] It is found that NBO dominates in determining the threshold of the O *K* edge; therefore, peak *B* in Fig. 1 can be assigned to the NBO peak. Similar results can be expected in the $ZnO\text{-}B_2O_3\text{-}SiO_2$ glass; i.e., peak *B* in Fig. 7 is due to the presences of the NBO's.

Based on Mott and Davis,[40] Fig. 12 schematically shows the origin of occupied and unoccupied states in silicate glasses. If an oxygen atom is bound to a single Si, it will have one unpaired electron in a nonbonding orbital. In silicate glasses, the cation is neutralized by an NBO in which

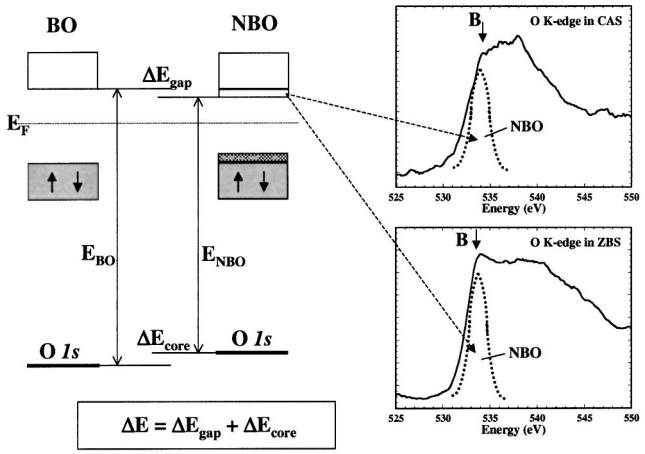

FIG. 13. Schematic drawing illustrating the shift of the threshold energy of the *K* edge between bridging and nonbridging O. The experimental data of the O *K* edges in the $CaO\text{-}Al_2O_3\text{-}SiO_2$ (CAS) and $ZnO\text{-}B_2O_3\text{-}SiO_2$ (ZBS) glasses are reproduced in the right panel.

the nonbonding orbital is occupied by two electrons. As a result, the top of the occupied and bottom of the unoccupied states should be sensitive to the presence of NBO's.

The formation of NBO by introducing cations into silicate glasses will cause the band gap to decrease.[41,42] Besides, the core levels ($1s$ and $2s$) of the NBO also shift upward (lower binding energy) compared with those of the BO.[43–45] This is schematically illustrated in Fig. 13. The common explanation given for this is that the higher effective valence charge is more localized on the NBO than that on the BO. Theoretical calculations show that more electron charge density occurs on an NBO than on a BO (Ref. 46). As shown in Fig. 13, the threshold energy in the EELS is determined by both the core-level energy and band gap;[47] therefore, the LDOS located on the NBO's should dominate the threshold of the O *K* edges in the glasses.

In situ EELS observations in this study found that the decay of the NBO peak occurs almost simultaneously with that of the cation (Ca and Zn in two glasses, respectively). This is consistent with the argument that the NBO's in the glass are associated with the cations. Elimination of the NBO by electron irradiation virtually results in threshold energy shifts of the O *K* edges toward higher binding energy. The threshold shift in the Ca aluminosilicate glass is about 2.1 eV. However, the threshold in the Zn borosilicate glass cannot be easily measured, because of the contribution from the increase of peak *C* (the π^* peak in trigonal *B*). In fact, the intensities of the NBO peaks (peak *B*) drop very quickly and eventually disappear. This suggests that the NBO's are weak links in the silicate network under electron irradiation. An electron-irradiation-induced decrease of NBO has been also observed by XPS study.[48] A similar correlation between the cation and NBO was also found in alkali silicate glasses under ion beam bombardment.[49]

In the intermediate stage of irradiation, the appearance and disappearance of peak *A* occur in both glasses. The interpretation of peak *A* must consider the fact that it is independent of the decay of NBO and cation. It is known that

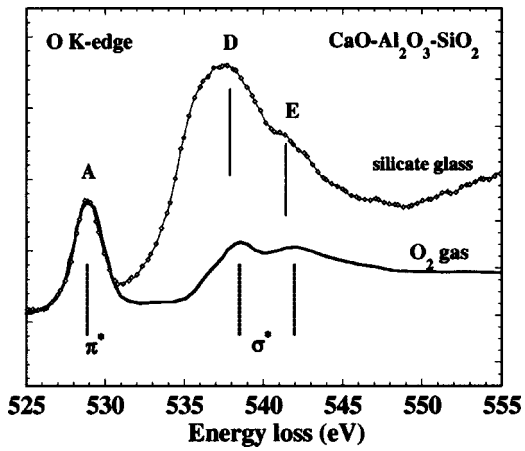

FIG. 14. Comparison of the O *K* edge in irradiated silicate glass with that from O_2 gas. The O *K* edge in O_2 gas is reproduced from Ruckman *et al.* (See Ref. 54).

many defects in silica or silicates can create unoccupied band-gap states.[50] Under electron irradiation, the NBO can become an isolated dangling-bonded oxygen site immediate after the removal of the cation. The hole(s) formed by creating dangling-bonded O_{NB}^{0} or O_{NB}^{+} may then lift the $p\pi$ nonbonding states above the valence-band top edge, which will be half or completely empty (Fig. 12).[54] In addition, two isolated dangling-bonded O_{NB} can easily form a peroxyl bond (O-O), which could also create unoccupied band-gap states depending on the charge(s) left in the peroxyl bond.[54] The densities of these defects should be dependent on the decay of the cation. However, peak *A* does not show such a direct correlation (Fig. 3). In contrast with the immediate decrease of the cation after electron irradiation, there is a delayed period before peak *A* is formed and then increases. Thus these O defects are unlikely to be responsible for the appearance of peak *A*. It should be noted that all of these defects might occur during electron irradiation, but one of the possible reasons for not seeing them in this study is the low efficiency of the currently used EELS detector. Under a low electron dose rate of illumination, these features may be buried in the high-background and dark-current noises. Under high dose rates, however, peak *A* may also cover these features.

As shown in Fig. 3, the intensity variation of peak *A* is similar to that of the total O intensity profile. Thus O diffusion into the illuminated region should be responsible for the creation of peak *A*. We suggest, therefore, that peak *A* should be related to the formation of molecular O_2 clusters or O_2 gas bubbles.

In the O_2 molecule clusters, the O $2p-$O $2p$ interaction creates O $2p\pi^*$ unoccupied (half filled) antibonding states in the band gap. Thus peak *A* can be assigned to the transition of the O $1s\rightarrow 2p\pi^*$. The spectra of the condensed and gas phase of O_2 have been studied previously, and there is a general agreement on the interpretation of the π^* peak.[51–54] For comparison, the energy positions of those major peaks in O_2 are reproduced in Fig. 14. Although there is controversy in interpreting $2p\sigma^*$ states, we can see that peaks *D* and *E* are in agreement with the transitions of the O $1s\rightarrow 2p\sigma^*$. This suggestion is consistent with the *in situ* EELS observations that show peak *A*, *D*, and *E* have same variation with electron irradiation (Table I). In the Zn borosilicate glass, however, the π^* peak in the O_2 is very weak: hence, the corresponding peak due to the σ^* cannot be recognized in the spectra.

B. Irradiation mechanisms

Generally, several mechanisms, such as knock-on, ionization, and field-induced migration, should be involved simultaneously in the interaction of high-energy electrons with solids. However, knock-on by the high-energy electrons cannot be the major interaction for those observed irradiation phenomena. For example, the Ca is the heaviest atom in the Ca aluminosilicate glass, but it is the only element to be driven out of the irradiation region during the initial electron irradiation. The ionization process is believed to be the dominant damage mechanism in the initial stage of irradiation. In addition, the temperature rise effects are also less important than the ionization damage.[2]

It is known that the region of the specimen under the center of the incident electron beam will be positively charged due to ionization.[55] Excited by the primary incident electrons, a large amount of secondary and Auger electrons can be generated in the irradiated region. The average ''lifetime'' of these generated electrons [10^{-4}–10^{0} sec (Ref. 56)] is much longer than the passing time of the incident electron through the sample [$\sim 10^{-15}$ (Ref. 57)] as well as the ionization time [$\sim 10^{-15}$ sec]. Electrical equilibrium cannot be quickly restored within an ionization process, and thus positive charge is rapidly built up in the electron-illuminated area. However, a dynamic equilibrium could eventually be established because of the attraction to secondary and/or Auger electrons.

In silicate glasses, the species with the highest ionicity based on the Pauling electronegativities[58] are the unstable under the electron irradiation, such as Ca in the CaO-Al_2O_3-SiO_2 and Zn in the ZnO-B_2O_3-SiO_2 glass. This is because a positive electric field can be generated by electron irradiation.[27] However, this cannot be simply considered as the only reason for irradiation damage. Based on the *in situ* EELS observations, the removal of Ca in the Ca aluminosilicate glass immediately induces changes in the Si L_{23} edge (both intensity and ELNES), but has little effects on the Al L_{23} edge (Fig. 6), although Ca is bound to both the Si and Al tetrahedra. We suggest, therefore, that instabilities of cations in silicate glasses should be associated with the localization of the DOS on the NBO's.

It is known that one of the features in disordered systems is the localization of the DOS—i.e., spatial confinement to the vicinity of predominantly a single atomic site, due to either the fluctuations in short-range order or the occurrence of short-range disorder in nonbonded atoms.[59,60] These localized states are more likely in the band tails.[61] NBO may also result in the localized DOS. Both experiments and theoretical calculations on sodium silicate glasses have confirmed the dominant O $2p$ contribution from NBO to the top of the occupied states.[62] These states are found to be highly local-

ized on the NBO (Ref. 63). According to the experiments on the drift mobility in a-SiO_2, Hughes reported that there was no charge transport due to the holes.[64] Based on the above knowledge, we believe that electron-irradiation-induced holes on the NBO's are highly localized and hence have reasonably long lifetimes. It should be noted that unlike the occupied states, the unoccupied states are not localized, which is also confirmed experimentally and theoretically.[65,66]

Here we suggest a modified Knotek-Feibelman mechanism[67] to explain that the double-ionization processes on the NBO's may enhance the instabilities of the cations under electron irradiation. In the original Knotek-Feibelman model, the intra-atomic and interatomic Auger decays of the core hole(s) may turn an anion into a positively charged ion and, thus, into a totally repulsive potential. However, the cations are seldom seen to move in the Knotek-Feibelman model.[68] For the sake of simplicity, we consider the configuration of Si-O_{NB}-M (M=Ca or Zn). Several Auger decay channels may create two holes in the NBO's. Excited by incident electrons, an O 1s or 2s (Refs. 69 and 70) core hole can be created, and the subsequent deexcitation process may result in the formation of two valence holes (one valence electron fills the O core hole and another is ejected as an Auger electron). In addition, the interatomic Auger decay from the transition of the valence electron of the O atom to the highest core hole in the cation could also accomplish double ionization of the NBO ion. As discussed above, these holes should be highly localized in the NBO's. In the configuration of the Si-O_{NB}-M, it is presumed that the Si-O_{NB} is the covalent bond, while the O_{NB}-M is an ionic bond, arising from electrostatic attraction. Once two holes are created on an O_{NB} and M bond, the attractive electrostatic force between the O_{NB}-M becomes repulsive. If the lifetime of the holes is long enough, which we believe from the localized states, the cation is released from the network. Driven by the repulsive electrostatic interaction, the breakaway Ca is easily removed from the electron-illuminated area. This is consistent with the experimental observations in Fig. 3 that only the EELS intensity of the Ca L_{23} edge decreases dramatically during the initial irradiation.

C. Diffusion of Si and O and the formation of O_2

Under electron irradiation, cations are driven away from their original sites. If the irradiated area is small, such as the use of a subnanometer probe in STEM, the cations will migrate into the adjacent region and leave a large amount of vacancies in the irradiated region. It should be noted that such diffusion processes are not driven by chemical potentials, but by repulsive electrostatic forces generated by the process of losing electrons in the irradiated region. From the microscopic point of view, the repulsive forces could be directly from the nearby NBO, which loses two electrons from the Auger process. From the macroscopic point of view, the repulsive forces could also come from the positive potential within the irradiated region.[27] Therefore, the vacancies left by cations are not necessary to be negatively or positively charged.

According to the *in situ* EELS observations, the EELS intensities of the Si L_{23} edges significantly increase during the initial stage of electron irradiation (Fig. 8). As shown in Fig. 3, the EELS intensity of the O K edge also has a slight increase at lower-dose-rate irradiation, but it becomes significant under higher dose rate (Fig. 6). This suggests that the cation vacancies can be partly filled by Si and partly by O. Once the Si fills the cation vacancies, the NBO's will be converted into BO's. This is confirmed by the experimental results that the tetrahedral characteristics of the ELNES of the Si L_{23} edge become more and more distinct within 20 sec of irradiation (Fig. 4). Once the O fills the cation vacancies, O_2 may form. Under this suggestion, the amount of O_2 clusters should be dependent on the amount of diffused O from the adjacent region. This is also consistent with what we have seen in the *in situ* EELS observations (Fig. 6). It should be noted that the transformation of NBO to BO and the formation of O_2 are processes that make the electron charge balanced. Under electron irradiation, such electron charge balances can be easily fulfilled locally by the absorption and emission of electrons through the dynamic processes of ionization and de-ionization.

It should be noted that the reaction of the diffused O from adjacent region with NBO's in the irradiated region is in competition with that of the diffused Si. However, the driving force for the diffusion is not clear at present. The O diffusion is probably caused by electrical attraction induced by electron irradiation, while exchange between Si and the cations might result in Si diffusion.[71] Under this assumption, O diffusion is much easier under high-dose irradiation than low dose. A relatively high O diffusion rate under high-dose irradiation results in the high intensity of EELS of the O_2 clusters.

Molecular O_2 might diffuse out from the surfaces into vacuum or segregate together to form O_2 clusters or even gas bubbles. These should be composition (i.e., NBO amount) and irradiation dose rate dependent. A dynamic equilibrium can be expected, thus resulting in the third (saturated) stage of irradiation observed in Fig. 3. Since the O_2 is formed by reaction of the diffused O with NBO, the amount of O_2 will decrease under further irradiation once the NBO's have been all consumed. As indicated in Fig. 6, beyond a certain time of irradiation, no O_2 can be detected no matter how long the sample is continuously exposed to electron irradiation.

D. Participation of metal particles and phase separation

The removed cations may capture secondary and/or Auger electrons and thus be neutralized into atoms with a certain kinetic energy. The nucleation and growth of cation particles may occur once the dimension of the accumulated cation atoms exceeds a critical value. So precipitation of the metal particles is also NBO dependent since the cations binding to NBO are likely to be removed. With larger amounts of NBO, a larger amount of cations can be released; hence, there is a higher chance to form particles. For example, we have observed the Zn particle precipitation from the ZnO-B_2O_3-SiO_2 in this study (Fig. 11).

In addition, the released cations may also fill the vacancies left by the Si that diffuse into the irradiated region. So there is also the possibility to form cation-O clusters, which

have been observed in a multicomponent alkaline-earth boroaluminosilicate glass.[72] Based on the *in situ* EELS observations and suggested mechanisms, electron irradiation has tendency to create a NBO free region, hence inducing separation of the glass phase into cation-rich and -poor regions.

V. CONCLUSIONS

In summary, cations, as glass network modifiers, along with the NBO's, are very sensitive to electron irradiation. This probably arises from the highly localized DOS on the NBO-cation bonds. A series of irradiation effects, in fact, are induced by the tendency to eliminate NBO's in the region under irradiation. Phase separation into cation-rich and -poor regions is thus an unavoidable trend for silicate glasses. During the reconstruction under irradiation, some of the NBO's are converted into BO's, with diffusion of Si (or B), while some form O_2 molecules or clusters, with diffusion of O. These various processes are in competition and depend on the irradiation rate and glass composition. At higher rates of irradiation, larger amounts of O_2 are formed. O_2 molecules or O_2 clusters may diffuse into vacuum from the surfaces during electron irradiation. As a result, a dynamic equilibrium of forming and losing O_2 may occur. Once the NBO's are all consumed, O_2 may eventually disappear into vacuum. The released cations may either fill the vacancies outside the irradiated region left by Si and form cation-rich region or capture free electrons created by electron irradiation and become neutralized atoms. Therefore the precipitation of metallic particles is also an expected product of irradiation. This is also dependent on the amount of NBO's. Eventually, there will be no NBO left in the irradiated region. Then the mechanisms introduced in this study will no longer dominate the irradiation effects in glass and other mechanisms must be considered.[73,74]

ACKNOWLEDGMENTS

This work was supported by the NSF through the Cornell Center for Materials Research (CCMR), which also supports the operation and maintenance of the STEM (NSF Grant No. DMR-9632275). One of the authors (N.J.) is also grateful to NSF Award No. DMR-0245702 for support. We thank Professor J. C. H. Spence of Arizona State University for a critical reading of the manuscript.

*Corresponding author. Electronic address: nan.Jiang@asu.edu

[1] D. Ehrt and W. Vogel, Nucl. Instrum. Methods Phys. Res. B **65**, 1 (1992).
[2] N. Jiang, J. Qiu, and J. Silcox, Appl. Phys. Lett. **77**, 3956 (2000).
[3] Y. Ito, H. Jain, and D. B. Williams, Appl. Phys. Lett. **75**, 3793 (1999).
[4] M. Yamane and Y. Asahara, *Glasses for Photonics* (Cambridge University Press, Cambridge, England, 2000).
[5] N. Jiang, J. Qiu, A. L. Gaeta, and J. Silcox, Appl. Phys. Lett. **80**, 2005 (2002).
[6] For a review and references see W. J. Weber *et al.*, J. Mater. Res. **12**, 1946 (1997).
[7] J. Todd, J. L. Lineweaver, and J. T. Kerr, J. Appl. Phys. **31**, 51 (1960); J. L. Lineweaver, *ibid.* **34**, 1789 (1963).
[8] J. F. DeNatale and D. G. Howitt, Nucl. Instrum. Methods Phys. Res. B **1**, 489 (1984).
[9] K. Awazu and H. Kawazoe, J. Non-Cryst. Solids **179**, 214 (1994).
[10] R. A. Kushner, D. V. McCaughan, V. T. Murphy, and J. A. Heilig, Phys. Rev. B **10**, 2632 (1974).
[11] A. Manara, M. Antonini, P. Camagni, and P. N. Gibbson, Nucl. Instrum. Methods Phys. Res. B **1**, 475 (1984).
[12] D. L. Griscom, J. Non-Cryst. Solids **6**, 275 (1971).
[13] D. L. Griscom, J. Non-Cryst. Solids **64**, 229 (1984).
[14] D. L. Griscom, M. E. Gingerich, and E. J. Friebele, Phys. Rev. Lett. **71**, 1019 (1993).
[15] M. A. Stevens-Kalceff, Phys. Rev. Lett. **84**, 3137 (2000).
[16] H. Jain and A. Sharma, Phys. Chem. Chem. Phys. **4**, 3232 (2002) and references therein.
[17] R. F. Egerton, *Electron Energy Loss Spectroscopy in the Electron Microscope* (Plenum, New York, 1996).
[18] J. Fink, in *Unoccupied Electronic States*, edited by J. C. Fuggle and J. E. Inglesfield (Springer-Verlag, Berlin, 1992), pp. 203–239.
[19] N. Jiang, J. Qiu, and J. C. H. Spence, Phys. Rev. B **66**, 054203 (2002).
[20] D. Weaire and M. F. Thorpe, Phys. Rev. B **4**, 2508 (1971).
[21] L. A. J. Garvie and P. R. Buseck, Am. Mineral. **84**, 946 (1999).
[22] R. P. Gupta, Phys. Rev. B **32**, 8278 (1988).
[23] E. J. Kirkland and M. Thomas, Ultramicroscopy **62**, 79 (1996).
[24] D. McMullan, P. Fallon, Y. Ito, and A. McGibbon, in *Proceedings of the 10th European Congress on Electron Microscopy—EUREM 92* (1992), Vol. 1, p. 103.
[25] E. Kirkland, Ultramicroscopy **32**, 349 (1990).
[26] J. I. Goldstein, J. L. Costley, G. W. Lorimer, and S. J. B. Reed, Scanning Microsc. **1**, 315 (1977); R. Hutchings, M. H. Loretto, I. P. Jones, and R. E. Smallman, Ultramicroscopy **3**, 401 (1979).
[27] J. Cazaux, Ultramicroscopy **60**, 411 (1995).
[28] Basically, the charging effects depend on the total positive charges trapped inside the electron-irradiated region. Using a subnanometer probe, it is easy to remove cations from the illuminated to the adjacent region (see Ref. 5 and the results of this work). Therefore, the trapped positive charges decrease. However, using a broad beam—for example, submicron probe—only the cations near the boundaries can be removed into an adjacent region. The remained cations may cause severe ''charging problems,'' such as sample drift.
[29] L. G. Parratt, Rev. Mod. Phys. **31**, 616 (1959).
[30] M. Inokuti, Rev. Mod. Phys. **43**, 297 (1971).
[31] D. A. Muller, D. J. Singh, and J. Silcox, Phys. Rev. B **57**, 8181 (1998).
[32] The decay rates are estimated by fitting the intensity curves of the ADF and Ca in Fig. 3 by $I(t)/I_0 = t^{-r}$, where t is irradiation time and thus r can be considered in the intensity decay rate. It is found that $r(\mathrm{Ca}) = 0.16 \gg r(\mathrm{ADF}) = 0.04$.
[33] V. J. Nithianandam and S. E. Schnatterly, Phys. Rev. B **38**, 5547 (1988).
[34] A. Bianconi, Surf. Sci. **89**, 41 (1979).
[35] T. A. Carlson, *Photoelectron and Auger Spectroscopy* (Plenum, New York, 1975).
[36] L. A. Garvie, A. J. Craven, and R. Brydson, Am. Mineral. **80**, 1132 (1995).

[37] H. Kawazoe, R. Suzuki, S. Inoue, and M. Yamane, J. Non-Cryst. Solids **111**, 16 (1989).
[38] *CRC Handbook of Chemistry and Physics*, 80th ed. (CRC Press, Cleveland, 2000), pp. 6–121.
[39] N. Jiang, Solid State Commun. **122**, 7 (2002).
[40] N. F. Mott and E. A. Davis, *Electronic Processes in Non-crystalline Materials* (Oxford University Press, New York, 1979), p. 515.
[41] For a review, see J. Wong and C. A. Angell, *Glass Structure by Spectroscopy* (Dekker, New York, 1976).
[42] T. Uchino, T. Sakka, Y. Ogata, and M. Iwasaki, J. Phys. Chem. **97**, 9642 (1993).
[43] R. Brückner, H.-U. Chun, and H. Goretzki, Glastech. Ber. **49**, 211 (1976); **51**, 1 (1978).
[44] Y. Miura, S. Matsumoto, T. Nanba, and T. Akazawa, Phys. Chem. Glasses **41**, 24 (2000).
[45] J. S. Jen and M. R. Kalinowski, J. Non-Cryst. Solids **38&39**, 21 (1989).
[46] Y. Kowada, H. Adachi, M. Tatsumisago, and T. Minami, J. Non-Cryst. Solids **177**, 286 (1994).
[47] R. D. Leapman, L. A. Grunes, and P. L. Fejes, Phys. Rev. B **26**, 614 (1982).
[48] R. K. Brow, J. Non-Cryst. Solids **175**, 155 (1994).
[49] R. K. Brow, J. Vac. Sci. Technol. A **7**, 1673 (1989).
[50] E. P. O'Reilly and J. Robertson, Phys. Rev. B **27**, 3780 (1983).
[51] A. P. Hitchcook and C. E. Brion, J. Electron Spectrosc. Relat. Phenom. **18**, 1 (1980).
[52] P. Kuiper and B. I. Dunlap, J. Chem. Phys. **100**, 4087 (1994).
[53] Y. Ma, C. T. Chen, G. Meigs, and K. Sette, Phys. Rev. A **44**, 1848 (1991).
[54] M. W. Ruckman, J. Chen, S. L. Qiu, P. Kuiper, M. Strongin, and B. I. Dunlap, Phys. Rev. Lett. **67**, 2533 (1991).
[55] C. J. Humphreys, T. J. Bullough, R. W. Devenish, D. M. Maher, and P. S. Turner, Scanning Microsc. Suppl. **4**, 185 (1990).
[56] The "lifetime" of the charged layers is estimated from (σ/ε), according to $\rho(t)=\rho(0)\exp(-[\sigma/\varepsilon]t)$, in which σ and ε are the conductivity and permittivity of the glass, and ρ is the charge density [D. J. Griffiths, *Introduction to Electrodynamics* (Prentice-Hall, Englewood Cliffs, NJ, 1981), p. 324]. For glasses, $\sigma=10^{-14}-10^{-10}\ (\Omega\,\mathrm{m})^{-1}$ [*Handbook of Chemistry and Physics*, 80th ed. (CRC Press, Cleveland, 2000)].
[57] An incident high-energy electron (100 keV) is passing through a specimen of several hundreds nanometer at the half of the light speed.
[58] L. Pauling, *The Nature of the Chemical Bond*, 3rd ed. (Cornell University Press, Ithaca, NY, 1960).
[59] P. W. Anderson, Phys. Rev. **109**, 1492 (1958).
[60] N. F. Mott, Philos. Mag. **35**, 111 (1977).
[61] S. R. Elliott, in *Physics of Amorphous Materials* (Longman Science and Technical, New York, 1990), pp. 281–300.
[62] W. Y. Ching, R. A. Murray, D. J. Lam, and B. W. Veal, Phys. Rev. B **28**, 4724 (1983).
[63] R. A. Murray and W. Y. Ching, J. Non-Cryst. Solids **94**, 144 (1987).
[64] R. C. Hughes, Appl. Phys. Lett. **26**, 436 (1975).
[65] R. C. Hughes, Phys. Rev. Lett. **30**, 1333 (1973).
[66] W. Y. Ching, Phys. Rev. B **26**, 6622 (1982).
[67] M. L. Knotek and P. J. Feibelman, Phys. Rev. Lett. **40**, 964 (1978); P. J. Feibelman and M. L. Knotek, Phys. Rev. B **18**, 6531 (1978).
[68] M. L. Knotek and P. J. Feibelman, Surf. Sci. **90**, 78 (1979).
[69] V. N. Ageev, Y. A. Kuznetsov, and T. E. Madey, Phys. Rev. B **58**, 2248 (1998).
[70] R. Souda, Phys. Rev. Lett. **82**, 1570 (1999).
[71] G. H. Frischat, in *Ionic Diffusion in Oxide Glasses*, Diffusion Monograph Series No. 3/4, edited by Y. Adda *et al.* (Trans. Tech. Publications, Bay Village, Ohio, 1975).
[72] N. Jiang and J. Silcox, J. Appl. Phys. **92**, 2310 (2002).
[73] L. W. Hobbs, Scanning Microsc. Suppl. **4**, 171 (1990).
[74] G. Chen, C. Boothroyd, and C. J. Humphreys, Appl. Phys. Lett. **62**, 1949 (1993).